Quantifying the diverse contributions of hierarchical muscle interactions to motor function

David O'Reilly[1]; William Shaw[1]; Pauline Hilt[2]; Rafael de Castro Aguiar[1]; Sarah L Astill[1]; Ioannis Delis[1]
[1]School of Biomedical sciences, University of Leeds, Leeds, United Kingdom.
[2] INSERM UMR1093-CAPS, Université Bourgogne Franche-Comté, UFR des Sciences du Sport, F-21000, Dijon, France.

Abstract

The muscle synergy concept suggests that the human motor system is organised into functional modules comprised of muscles '*working together'* towards common task-goals. However, recent innovative work has added further nuance to this idea, showing how muscles may also work together towards functionally different and independent task-goals, representing crucial attributes of flexible motor behaviour. Here we probed this proposed functional neural architecture by building upon an established theoretical framework to characterise distinct types of muscle interactions, i.e. functionally similar, complementary and independent, across scales. Through a novel application of the Partial Information Decomposition to large-scale muscle activations, we unveiled complex networks of inter- and intra-muscular interactions with distinct functional roles as well as independent muscle contributions to task performance. We showcased the effectiveness of this approach by extracting hierarchical and functionally diverse motor components that were a) generalisable across participants and tasks and b) predictive of balance performance across trials and of differences in motor variability between young and older adults. In aligning muscle synergy analysis with the forefront of understanding on human movement modularity, our findings suggest the proposed methodology can offer novel biological insights into the neural control of movement and research opportunities towards health and engineering applications.

Introduction

Hierarchical modularity is a ubiquitous characteristic of complex living systems such as the human nervous system [1,2]. The constituent parts (i.e. individual neurons, muscles etc.) at each level interact in a goal-directed manner [3], forming functionally specialized modules that cooperate towards common task-goals. The putative interactions within these modules include a common selectivity (i.e. redundancy) for task information along with unique contributions by individual parts to the processing of task information. To exemplify this point in the context of motor control, in seminal work Ivanenko and colleagues noted: "*…We can think of (*electromyographic*) EMG waveforms as being dependent on two aspects. First, there are some underlying common waveforms shared by the muscles. Second, each muscle also captures a unique aspect of activation that is not addressed by any other muscle"* [4]. However, for a set of muscle activity patterns to form an emergent whole (i.e. a coordinated movement), the integration of redundant and unique muscle constituents in the form of cross-module, synergistic muscle interactions is necessary. Synergistic interactions combine information across functionally heterogeneous modules, therefore serving as important channels of communication for the integration of information in the nervous system [5,6]. The complementary information generated by these interactions is super-additive, emerging from the union of lower-level constituents [7]. Indeed, from a more coarse-grained view, these emergent functional modules themselves, through hierarchies of complementary interactions [8], form parts of greater wholes (i.e. submodules-within-modules) [9].

Motor control research, has focused primarily on deciphering how the many redundant degrees-of-freedom of the human body are coordinated for everyday tasks [10,11]. This avenue of research uses the '*muscle synergy'* as a guiding concept [12,13], where the cohesive interactions between groups of muscles ('*muscle synergies'*) map to common task-goals, and in doing so simplify movement execution. Recent influential works however suggest that a more nuanced functional architecture underlies human motor control [14–17]. For instance, anatomically proximal musculature thought to have equivalent task efficacy have, in fact, demonstrated a partial decoupling and sharing of common drive with distal musculature [14,15]. Moreover, the identification of independent functional modules indicates that multiple sources of common drive are present in the muscle space [17]. Altogether, this recent perspective proposes that functional modularity exists both between and within muscles, simplifying the control of movement by enabling the flexible compliance of muscles towards multiple task-objectives [18]. It is prescient for the field to develop new analytical approaches to comprehensively understand human movement modularity from this new perspective.

In [19], we addressed this research gap by proposing a computational framework that dissects task information into task-irrelevant (i.e. present across all tasks), -redundant (functionally similar) and -synergistic (functionally complementary) muscular interactions. In doing so, we aligned current analytical approaches with this novel perspective of flexible motor control. However, the separate quantification of the task-relevant information that is not shared or complementary between muscles (i.e. provided uniquely by a muscle), is not possible using current analytical approaches. Intuitively, this task

information encodes the functionally independent muscle activations that contribute uniquely to task performance, generated potentially by both central and peripheral sources [4,18,20]. Although independent motor control mechanisms are well-established and can improve with training [21,22], the inclusion of this attribute in recent theoretical work marks a significant departure from traditional perspectives [18]. Thus, here we will address an important current research gap by developing a methodology for the comprehensive quantification of unique task information in the muscle space.

A second consideration we address here concerns the coverage given by the muscle synergy concept to the contribution of whole muscle groups, rather than individual muscles, towards task-objectives. The motor redundancy problem motivating this concept describes how common neural inputs map to the task space through inter-muscular components [13]. However, the end-effectors of this mapping operation are in fact individual muscles with their own unique anatomical attachments and activation timings [16,23], thus, as recognized by several lines of recent research [9,15,18,24], the muscle group may not be the smallest unit of modular control. Only more recently has the muscle synergy concept been formally applied at the intramuscular level [24], revealing that intramuscular synergies are independent of the muscles' compartmentalized structure and may be complementary to inter-muscular analyses as a window into the neural control of movement [25,26].

In the current study, through a principled methodology, we aimed to probe the hierarchically structured functional architecture of the motor system, revealing salient features of movement modularity at multiple scales. To this end, we built upon traditional approaches by directly including task parameters during muscle synergy extraction but here, as a first for the field, by employing a partial information decomposition (PID) (Fig.1.1). With this novel implementation into an established pipeline (Fig.1.2), we can separately quantify redundant, synergistic, and unique task information. Intuitively, synergistic information (orange shaded area (Fig.1.1) and orange bar (Fig.1.2)) is the information shared by a given muscle pair ($[m_x, m_y]$) about a task parameter (τ) that can only be gained by observing m_x and m_y together. On the other hand, redundant information (pink intersection (Fig.1.1)) and pink bar (Fig.1.2)) is the task information shared by m_x and m_y that can be found in either alone. Finally, unique information (magenta and cyan intersections and bars in fig.1.1-2 respectively) is the task information provided by either m_x or m_y that is not found in the other.

Towards this aim, we applied the framework to three datasets of human movement (whole-body reaching – Dataset1, balancing on a balance board – Dataset2 and an object lifting task – Dataset3), revealing generalizable patterns of diverse task information processing both between and within muscles that encode distinct features of motor behavior. To supplement the work presented here, we provided Matlab code for readers to apply this framework to their own data: https://github.com/DelisLab/Muscle_PID.

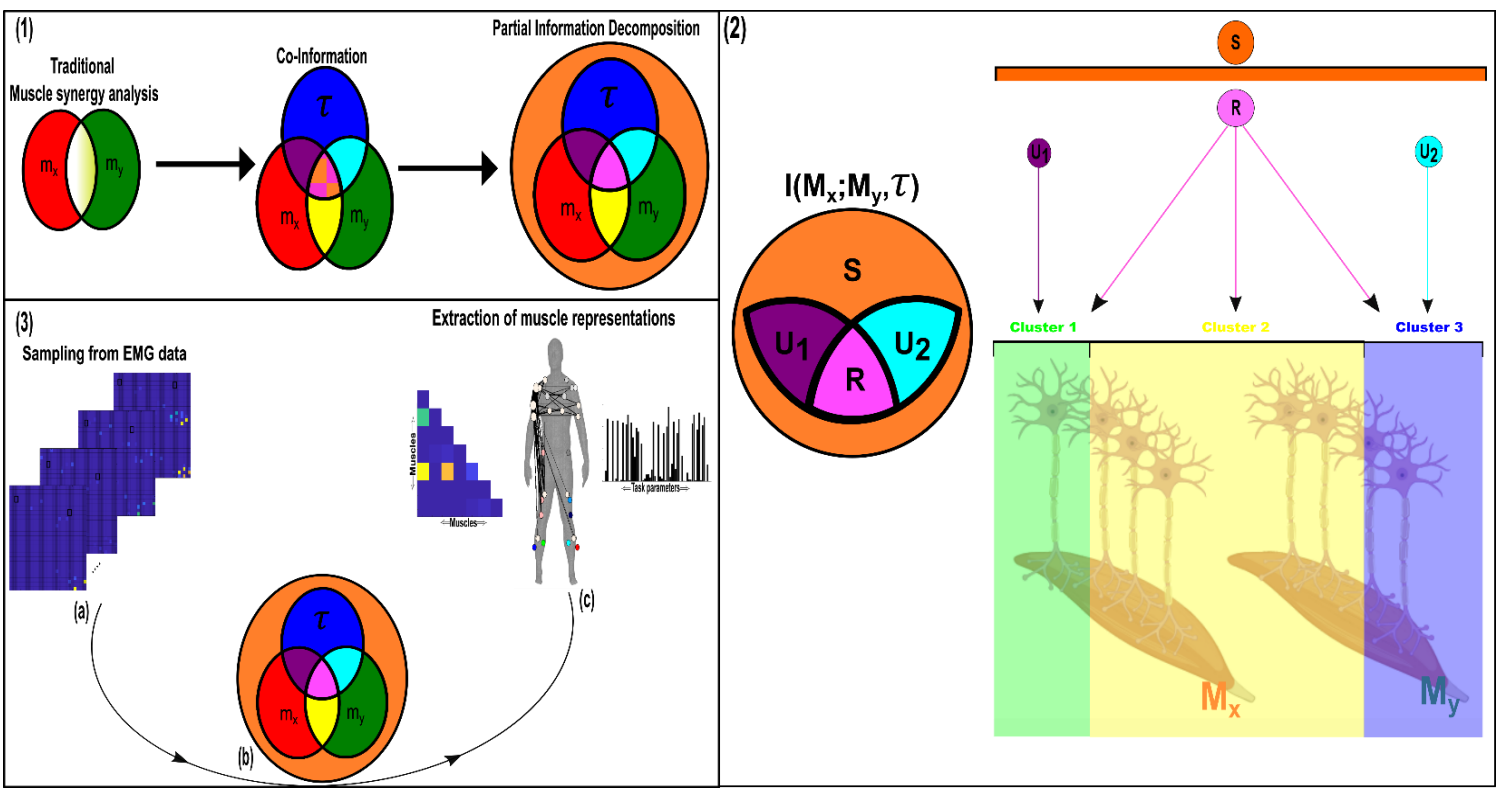

Fig.1: **(1)** Building on traditional muscle synergy analysis based on dimensionality reduction and a recent computational framework introducing an information-theoretic measure of net redundancy/synergy (pink-orange intersection) known as Co-Information [27], here we introduce Partial Information Decomposition (PID) [28] to quantify and functionally characterize muscle interactions. By employing

PID, we introduce the novel capability of separately quantifying redundant (pink intersection), synergistic (orange shaded area) and unique information (magenta and cyan intersections) from a given muscle pair ($[\mathbf{m_x}, \mathbf{m_y}]$) about a task parameter ($\boldsymbol{\tau}$). **(2)** This innovation aligns with theoretical developments on movement modularity by enabling the principled decomposition of their shared information ($\mathbf{I}(\mathbf{m_x}, \mathbf{m_y}; \boldsymbol{\tau})$) (see Equation 1.2 of Materials and methods section) into four non-negative quantities representing the functionally redundant, ($\mathbf{R}$), synergistic ($\mathbf{S}$) and unique ($\boldsymbol{U_1}$,$\boldsymbol{U_2}$) information components [18]. **(3)** An overview of the proposed framework. (**a**) EMG data along with corresponding task parameters are recorded from human participants performing naturalistic movements. (**b**) PID is applied to all $[m_x, m_y]$ and τ combinations, with the resulting information atoms then input into an established pipeline [19,29]. (**c**) The output of this framework is low-dimensional components consisting of pairwise dependencies between muscles and their task- and participant-specific activations.

Results

Our primary aim here is to probe the functional architecture of the motor system by establishing a principled method for quantifying task-redundant, -synergistic and unique informational dynamics underlying motor behavior. To achieve this, we firstly develop a novel computational framework and apply it to pairs of EMG signals across time ($[m_x, m_y]$) and a corresponding, continuous task parameter (τ) (e.g. kinematics, dynamics etc.) (see '*Quantifying functionally diverse muscular interactions'* section in the Materials and methods) [28]. The proposed Partial Information Decomposition (PID) framework parses the effects on τ by a pair of muscle activations ($[m_x, m_y]$) into four separate atoms of information (i.e. task-redundant (R), -synergistic (S) and two unique information components (U_x and U_y)) by decomposing their joint mutual information (JMI). R is the predictive information between $[m_x, m_y]$ about τ that can be found in either alone (sub-additive task information), encapsulating the portion of the $[m_x, m_y]$ pairing that has a similar functional consequence. S on the other hand, is the predictive information provided by $[m_x, m_y]$ about τ that is produced only when m_x and m_y are observed together (super-additive task information), capturing the functional complementarity within the interaction. Finally, U_x and U_y is the predictive information within $[m_x, m_y]$ about τ that is only present in m_x or m_y alone, capturing the unique contributions of the individual muscles within the functional interaction.

Following this decomposition, we then ran these separate PID atoms through an established pipeline [19,29], referred to as the Network-Information framework (NIF) (Fig.2(A-E)) (see Materials and methods for detailed breakdown). The purpose of the NIF is to produce functionally and physiologically relevant and interpretable low-dimensional components of muscular interactions underlying coordinated movements. The following briefly summarizes the main steps of the pipeline:

1. To produce a comprehensive network of functional muscle interactions, we applied the PID framework over all unique $[m_x, m_y]$ and τ combinations for each participant (Fig.2(B)). This iterative procedure results in a multiplex network, with each layer consisting of all functional dependencies between muscle pairs for a particular PID atom, τ and participant.
2. To determine the statistically significant interactions, we applied a modified percolation analysis to each layer of the multiplex network (Fig.2(C)) [6].
3. To determine the optimal number of clusters to extract from structurally nested networks, we employed a link-based community detection protocol based on a modularity maximization cost-function (Fig.2(D)) [30–32].
4. The optimal cluster count was then used as the input parameter into dimensionality reduction, namely a projective non-negative matrix factorization (PNMF) algorithm [33], to extract patterns of muscle connectivity along with their task- and participant-specific activations (Fig.2(E)).

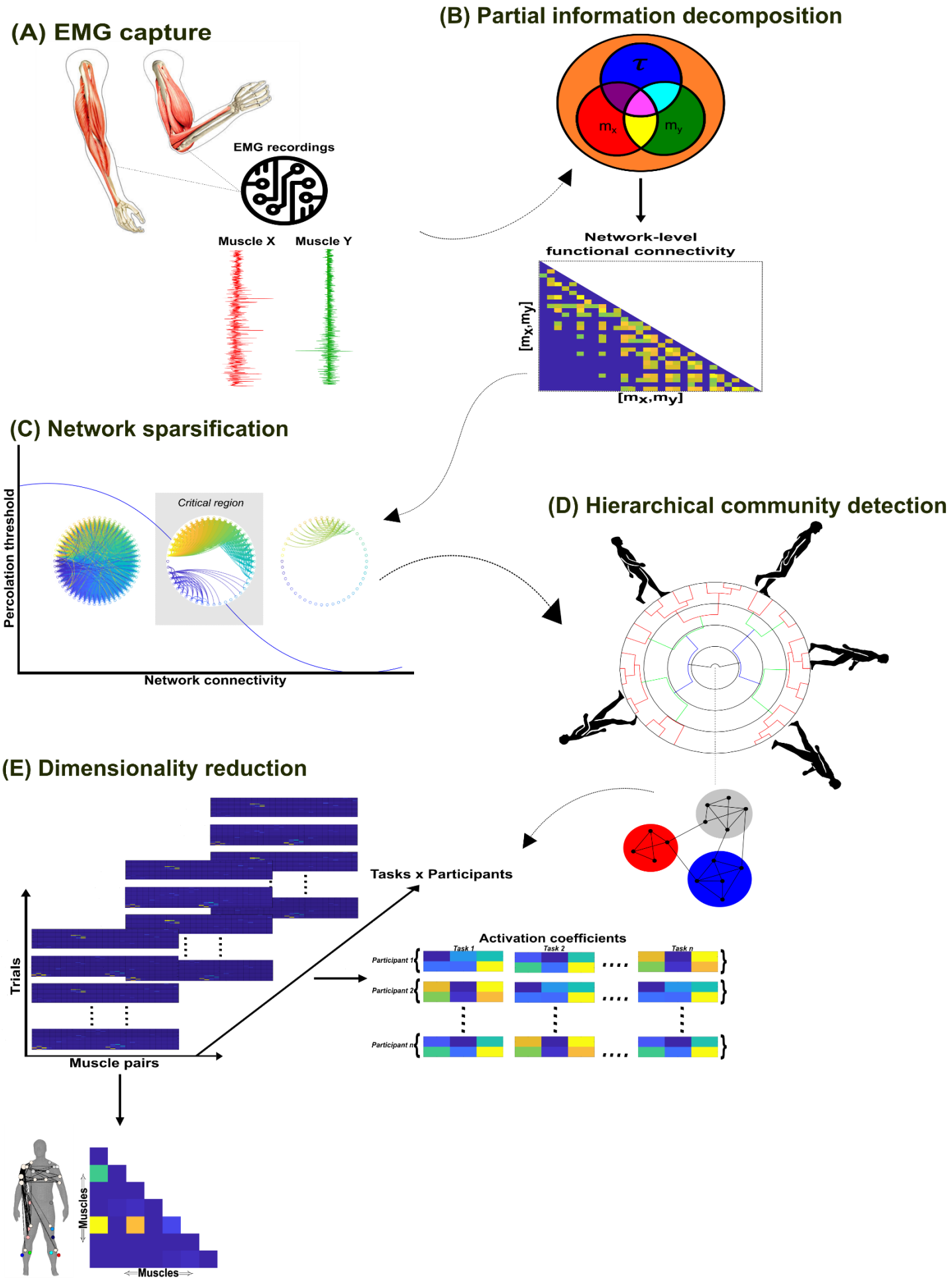
(A) EMG capture
EMG recordings
Muscle X
Muscle Y
(B) Partial information decomposition
τ
m_x
m_y
Network-level functional connectivity
$[m_x,m_y]$
$[m_x,m_y]$
(C) Network sparsification
Critical region
Percolation threshold
Network connectivity
(D) Hierarchical community detection
(E) Dimensionality reduction
Trials
Muscle pairs
Tasks x Participants
Activation coefficients
Task 1
Task 2
Task n
Participant 1
Participant 2
Participant n
Muscles
Muscles

Fig.2: A summarized overview of the NIF pipeline. **(A)** EMG data is captured from human participants performing naturalistic movements. **(B)** The joint mutual information (JMI) between all muscle pair and continuous task parameter combinations is decomposed using the partial information decomposition framework, resulting in separate networks of redundant, synergistic, and unique muscle interactions. **(C)** Each network is sparsified with respect to its percolation threshold, identifying statistically significant functional connections. **(D)** A novel hierarchical community detection essentially unravels and identifies overlapping clusters of network dependencies. **(E)** The optimal number of clusters identified serves as the input parameter into dimensionality reduction, where low-dimensional components of muscular interactions along with task- and participant-specific activations are extracted.

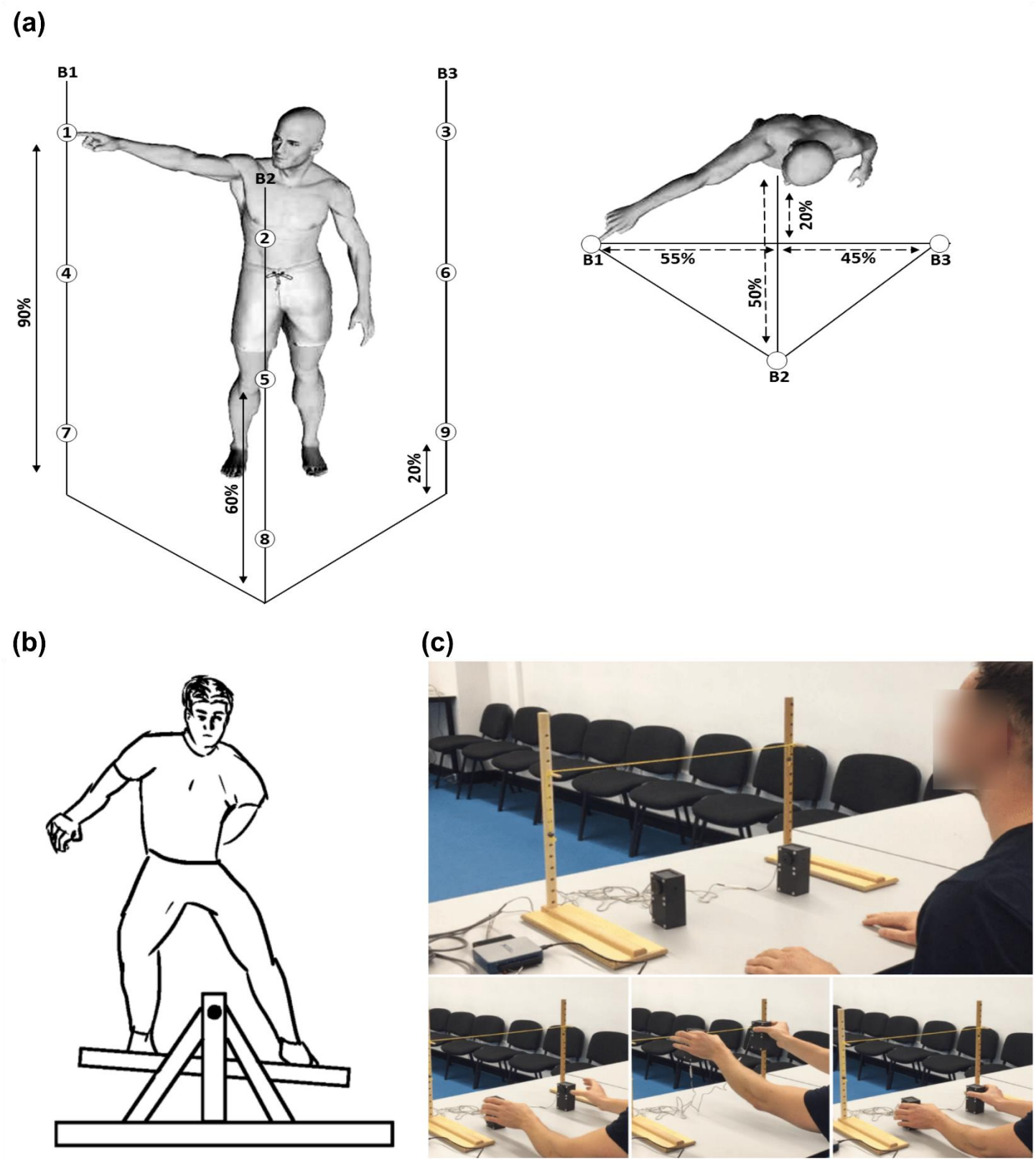

Fig.3: The datasets used in the application of the proposed framework in the current study. **(a) Dataset 1:** Healthy adult participants performed whole-body reaching tasks in various heights and directions while EMG and kinematics were captured across the body [34]. **(b) Dataset 2:** Healthy adult participants performed 10 trials of balancing on a balance board while EMG was captured among the bilateral lower-limb flexors and extensors simultaneously to the horizontal angular displacement of the balance board. **(c) Dataset 3:** Healthy younger and older adults performed a reach-grasp-lift-hold and replace task of both light and heavy objects while EMG from the arm musculature bilaterally were captured along with load and grip forces on the grasped object [35]. For full details on the experimental setup of these datasets, see *'Data acquisition and experimental conditions'* section of the Materials and methods.

Hierarchical and functionally diverse muscular interactions underly motor behavior

To demonstrate the proposed PID approach, we present an example output from an application to the EMG recordings of a single participant (across all trials) from Dataset 1 with respect to the reaching finger anterior-posterior kinematic coordinate. This participant was instructed to perform a total of 72 different randomly selected whole-body point-to-point reaching tasks for ~2160 trials (see fig.3(a)) and *'Data acquisition and experimental conditions'* section of the Materials and methods section). In fig.4, we illustrate the redundant (R – 4b), synergistic (S - 4c), and unique (U_x and U_y - 4d) interactions between muscles, as well as their sum total which they are all normalized by, (i.e. JMI -4a). Human body models accompanying each of the JMI, R and S muscle networks illustrate the strongest interactions between muscles (indicated by edge-width) [36], the muscle subnetworks (node color) and the network centrality (a measure of a muscle's relative importance indicated by node size) (see '*Subnetwork analysis'* section of Materials and methods) [30,37,38]. The U_x and U_y terms are not considered as a muscle coupling, as they encode the task information present in one muscle that is not present in another and vice versa, and so instead the average unique information (U_{xy}) for each muscle is presented as a bar graph.

The JMI network contains several reaching arm muscles including the anterior- and posterior deltoid and biceps and triceps brachii that form anatomically defined subnetworks (red and blue nodes) with multiple contralateral upper-limb and bilateral lower-limb muscles in the anterior-posterior direction (fig.4(a)). When these dependencies are decomposed into their PID components (fig.4(b-d)), we reveal a more complex functional architecture underlying whole-body reaching movements. These functionally diverse components consist of multiple subnetworks widespread across the body that are driven by prime-mover muscles such as the right biceps brachii and trapezius (fig.4(b-c)). Interestingly, these prime-movers did not contain much unique task information (fig.4(d)), while muscles displaying considerable functional independence did not feature prominently in the redundant and synergistic networks (e.g. right triceps brachii, anterior and posterior deltoid), indicating that the PID approach characterized distinct muscle networks with different functional roles.

Next, to elucidate the functional interactions within muscles underlying whole-body reaching movements, we applied the proposed methodology to pairwise combinations of amplitude signals from six frequency-bands ($[f_x, f_y]$) (Delta [0.1-4 Hz], Theta [4-8 Hz], Alpha [8-12 Hz], Beta [12-30 Hz], Low-Gamma (Piper rhythm) [30-60 Hz], High Gamma (Gamma) [60-80 Hz]) (see '*Quantifying diverse muscular interactions in the task space'* and '*Data pre-processing'* sections of the Materials and methods) extracted from the right anterior deltoid muscle. This computation serves as a novel, nonlinear measure of coherence decomposed into its task-relevant informational constituents, which we used here to determine the multifarious effects of $[f_x, f_y]$ on the right, reaching finger anteroposterior kinematic (Fig.5). The intramuscular JMI network comprised of a mixture of dependencies between distinct oscillations (Fig.5(a)), most prominently between the Delta-Theta rhythms. When we decomposed their shared task information, the rhythmic activities of the right anterior deltoid presented a more distinguishable encoding of task performance. Gamma amplitudes were functionally similar in their encoding of the finger kinematic with respect to all other frequency bands while a separate Delta-Theta coupling was also had functionally similar consequences (Fig.5(b)). The Piper rhythm comprised of task-synergistic information in the anterior deltoid muscle when coupled with the Theta and Alpha oscillations (Fig.5(c)). Meanwhile, the amplitude of beta oscillations provided the most functionally independent information about the reaching finger kinematic on average, followed by Delta and Theta amplitudes (Fig.5(d)).

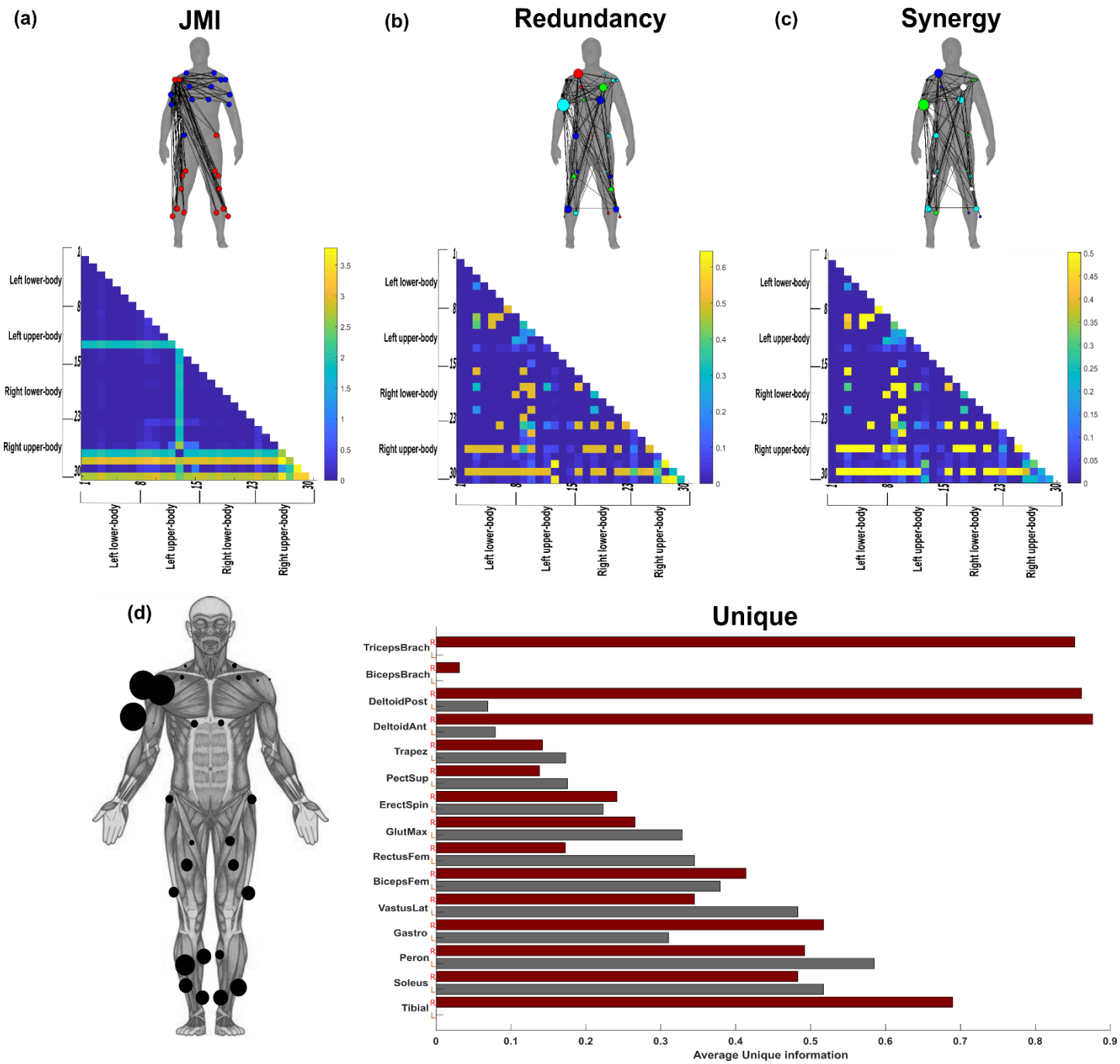

Fig.4: Application of the proposed framework to the intermuscular space of a single participant performing multiple trials of various whole-body reaching tasks (dataset 1). The Joint mutual information (JMI) **(a)** and its informational components**,** redundant **(b)**, synergistic **(c)** and unique information **(d)** were determined with respect to the reaching finger anterior-posterior kinematic coordinate. Values for R, S and U_{xy} were normalised with respect to the presented JMI values [39]. Human body models accompanying each representation in **(a)-(c)** illustrate the strongest connectivities (edge-width) [36], the subnetwork community structure (node color) and network centrality (relative node size) [30,37,38]. The U_x and U_y terms are not considered as a muscle coupling, as they encode the task information present in one muscle that is not present in another and vice versa, and so instead the average unique information (U_{xy}) for each muscle (left-side=grey, right-side=maroon) is presented as a bar graph. The accompanying human body model to the left illustrates the predominant muscles (black nodes) that encoded unique information about the right, reaching finger kinematic.

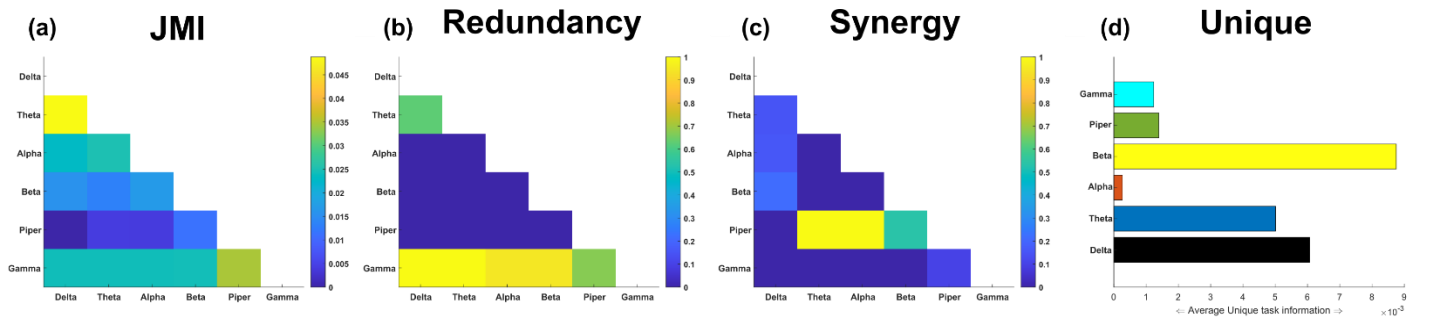

Fig.5: Application of the proposed framework to frequency-specific amplitudes in the reaching side anterior deltoid muscle of a single participant performing multiple trials of various whole-body reaching tasks (Dataset1). The Joint mutual information (JMI) **(a)** and its informational components**,** redundant **(b)**, synergistic **(c)** and unique information **(d)** were determined with respect to the reaching finger anterior-posterior kinematic coordinate. Values for R, S and U_{xy} were normalised with respect to the presented JMI values [39]. The U_x and U_y terms are not considered as a coupling, as they encode the task information present in one oscillation that is not present in another and vice versa, and so instead the average unique information (U_{xy}) for each frequency-band are presented together as a bar graph.

Generalizable components of functionally diverse inter- and intra-muscular interactions

Having demonstrated the presence of the parallel processing of R, S and U_{xy} between and within muscles, we then sought to extract motor components that are generalizable beyond any individual participant and task.

Beginning with intermuscular components, we identified four R and S (R1-R4 and S1-S4) and three U_{xy} (U1-U3) components with respect to the XYZ (anterior-posterior, medio-lateral vertical directions) coordinates of 21 kinematic markers (21 x 3 dimensions = 63 task parameters in total) across the body of three participants performing whole-body reaching movements (>2000 trials each). For brevity here, we provide illustrations of the output in the supplementary materials (Supp. Fig.1-3). To examine the generalizability of these components, we removed an individual task parameter or participant from the input data and then re-extracted the same number of components and computed the average correlation between corresponding components (see *'Examining the generalizability of the extracted components'* section of the Materials and methods). We found an almost perfect concordance between the presented intermuscular components and those extracted from a subset of the data (~0.99 average correlation). The robustness of these components exceeds previous implementations of the NIF [19,29], where a high level of concordance was also found.

Turning to the intramuscular space, applying the proposed approach within all 30 muscles with respect to 63 kinematic coordinates from the three participants of Dataset 1 revealed four R (R1-R4 (Supp. fig.4)) and three S (S1-S3, (Supp. Fig.5)) and U_{xy} (U1-U3 (Supp. fig.6)) components. The generalizability of these intramuscular components was proven at the intramuscular level with ~0.99 correlation typically for both individual tasks and participants among R and S networks. A slightly lower concordance among U_{xy} (r=0.9) was found when an individual participant was removed from the input data.

Hierarchies of functional muscle interactions encode distinct motor features

Finally, having established the presence of functional modularity and diverse task information processing across scales of muscular interactions, we then investigated the functional relevance of the extracted muscle networks. Specifically, we asked if the identified muscle interactions are predictive of motor performance (balance – Dataset2) and motor decline with age (object lifting – Dataset3).

Functionally diverse intermuscular interactions reflect balance performance

To begin with dataset 2, we identified and extracted five R, four S and four U_{xy} intermuscular components. We then used the trial-specific activations from the extracted components for each participant (normalized with respect to their corresponding JMI) to predict motor performance in each trial (i.e. the total balance board error calculated as the sum of absolute deviations from 0 degrees on the horizontal plane of the balance board) (∑Error) (see '*Salient features of motor performance'* of the Materials and methods section). As multiple observations for the same participant were present within these vectors (n=10 trials each), we determined associations using repeated measures correlation [40], a measure of linear correlation that models participant-specific clustering in the data.

We found two intermuscular interactions (S2 with synergistic couplings between both BF-R and MGN-R, and the left tibialis anterior (TA-L), r=0.638489, p=0.000256 and R2 with redundant couplings between the right medial-gastrocnemius (MGN-R) and biceps femoris (BF-R) and BF-R and left rectus femoris (RF-L), r=0.638489, p=0.000256) (Fig.6(A)). Interestingly, muscle couplings representing redundant and synergistic interactions here did not appear

prominently in the motor component U4 contributing uniquely to task performance. In contrast, the unique task information in the right rectus femoris (RF-R) and to a lesser extent TA-L (together possibly representing their important roles in crossed-extensor reflex actions) was related to a significant reduction in ∑Error (r=-0.438393, p= 0.019621), i.e. predicting better balance performance (Fig.6(A)).

Functionally similar intramuscular interactions reflect balance performance

Turning to the intramuscular space, we identified and extracted five R and three S and U_{xy} from Dataset2 and found three of these components significantly correlated with ∑Error across trials (see '*Salient features of motor performance'* of the Materials and methods section) (Fig.6(B)). These components all represented redundant amplitude couplings (R2-R4), consisting exclusively of specific coherences between the gamma band and other lower frequency amplitudes (delta and theta in R2, beta and piper in R3 and, alpha in R4), and were negatively correlated with ∑Error (i.e. increased involvement of intramuscular modules resulted in improved balance performance, r=-0.454, p=0.0153 for R2, r=-0.509, p=0.005665 for R3, and r=0.415, p=0.0282 for R4).

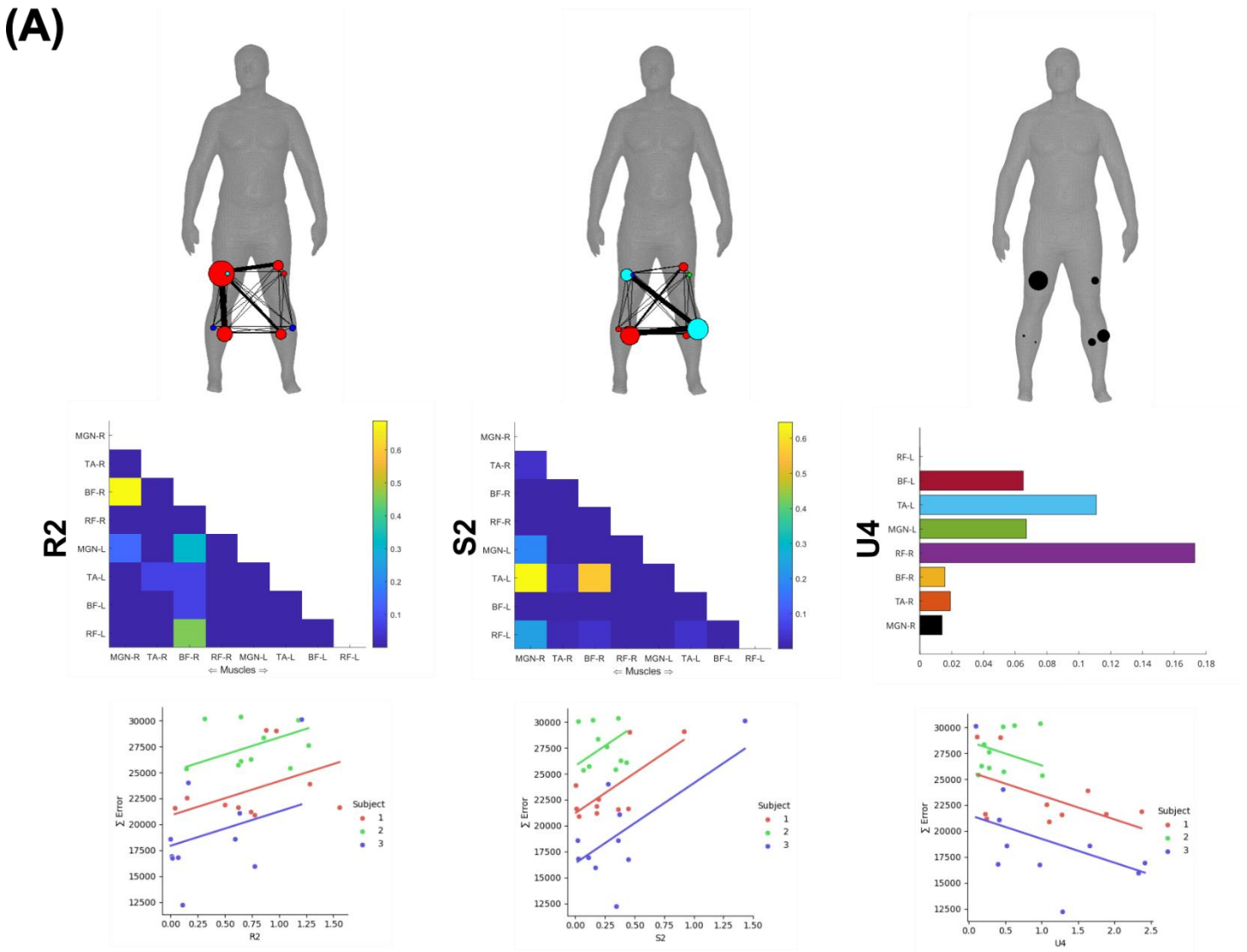
(A)
R2
S2
U4
MGN-R
TA-R
BF-R
RF-R
MGN-L
TA-L
BF-L
RF-L
⇐ Muscles ⇒
Σ Error
Subject
1
2
3

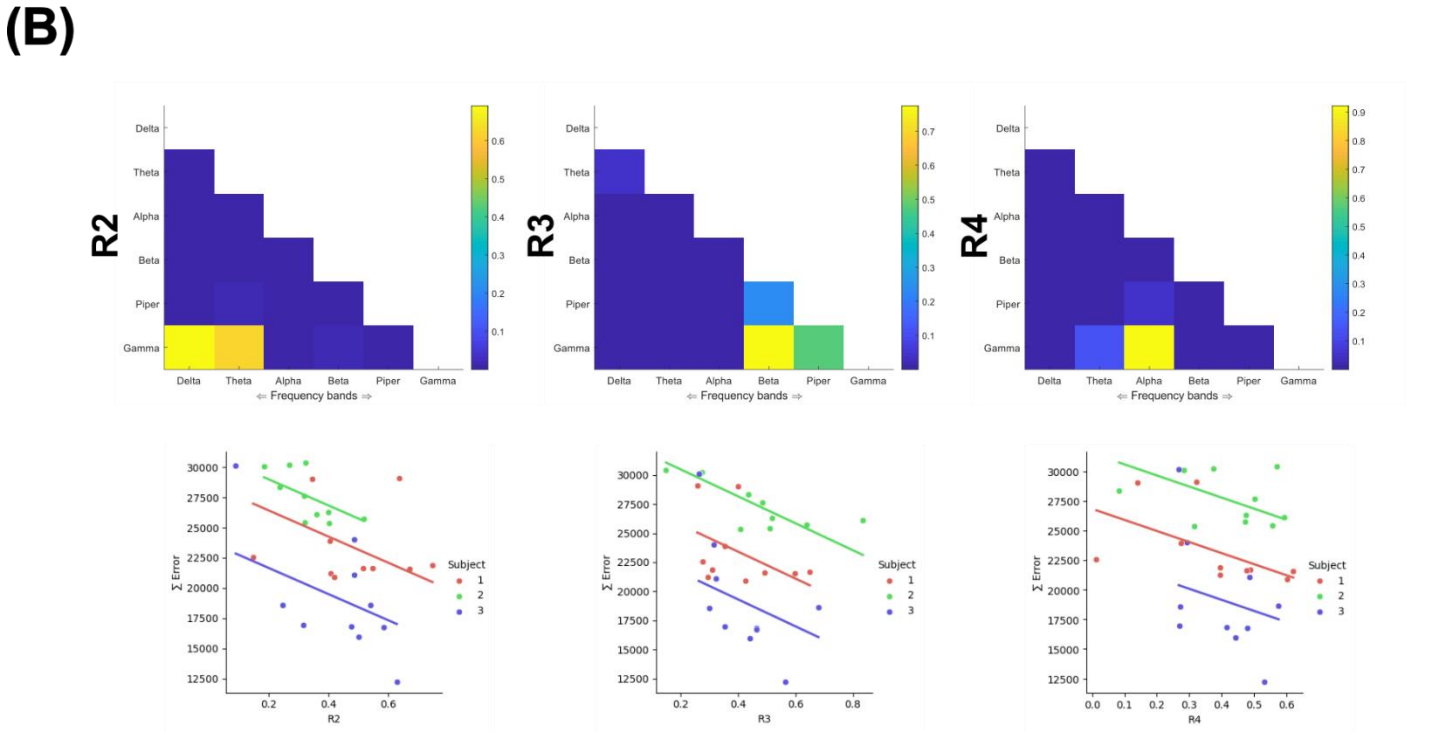
(B)
R2
R3
R4
Delta
Theta
Alpha
Beta
Piper
Gamma
⇐ Frequency bands ⇒
Σ Error
Subject
1
2
3

Fig.6: **(A)** The intermuscular components (R2, S2 and U4) determined to have a significant (P<0.05) correlation with balance performance (∑Error) across trials in Dataset2. Top: each adjacency matrix, the human body models illustrate the network structure with relative edge thickness, node size and color reflecting connection strength, importance and sub-modularity respectively [30,37,38]. Bottom: Scatterplots illustrating the corresponding repeated measures correlation with balance performance. **(B)** Top: The intramuscular components (R2, R3 and R4) determined to have a significant (P<0.05) correlation with balance performance (∑Error) across trials in dataset 2. Bottom: Scatterplot of the corresponding repeated measures correlation outputs.

A combination of bilateral muscle networks predicts age differences in bimanual object-lifting

Next, we asked which muscle interactions may underpin differences in motor performance resulting from ageing. In the motor control literature, older adults have been shown to exhibit greater motor variability compared to young cohorts [41], leading to behavioral inconsistency. To answer this question, we applied our proposed approach to Dataset 3 [35], consisting of EMG recordings (8 upper-limb muscles bilaterally) from healthy young (N=14) and older (N=18) participants performing a bimanual reach-grasp-hold task of both light and heavy objects (see fig.3(c) and '*Data acquisition and experimental conditions'* section of the Materials and methods).

Applying PID to all pairs of EMG signals to predict the bilateral grip and load forces (i.e. 4 task parameters) the participants exerted, we identified and extracted five R, seven S and three U_{xy} intermuscular components. To investigate how this variability would manifest in the extracted functional muscle patterns, we defined a measure of motor variability in the activation of muscle or frequency couplings (∑Error) and applied it to the extracted components (see *'Salient features of motor performance'* of the Materials and methods section). These vectors were then employed as the predictors in a binary logistic regression model against participants' age group (Young=0 vs. Old=1). This procedure indicated that a combination of the 5th R (β= -2.12±0.801, p<0.01), 7th S (β= 1.36±0.704, p=0.053) and 3rd U_{xy} (β= 0.964±0.445, p<0.05) motor components were optimal in predicting age group (Fig.7(A)), classifying 75% of participants correctly.

A combination of functionally diverse intramuscular rhythms predict age differences in bimanual object-lifting

When applied in the same way to the corresponding intramuscular level of Dataset3, we identified and extracted five R, four S and four U_{xy} rhythmic components. Participants' age group was optimally predicted by a combination of the 4th R (β= -0.557±0.313, p=0.075), the 2nd S (β= -11.75±4.6, p=0.011) and the 1st U_{xy} (β= 1.94±0.982, p<0.05), which classified 84.4% of participants correctly (Fig.7(B)). Taken together, these findings suggest that concomitant increases and decreases in the fluctuations of functionally diverse muscle interactions across scales characterize aging-induced changes in upper limb motor function.

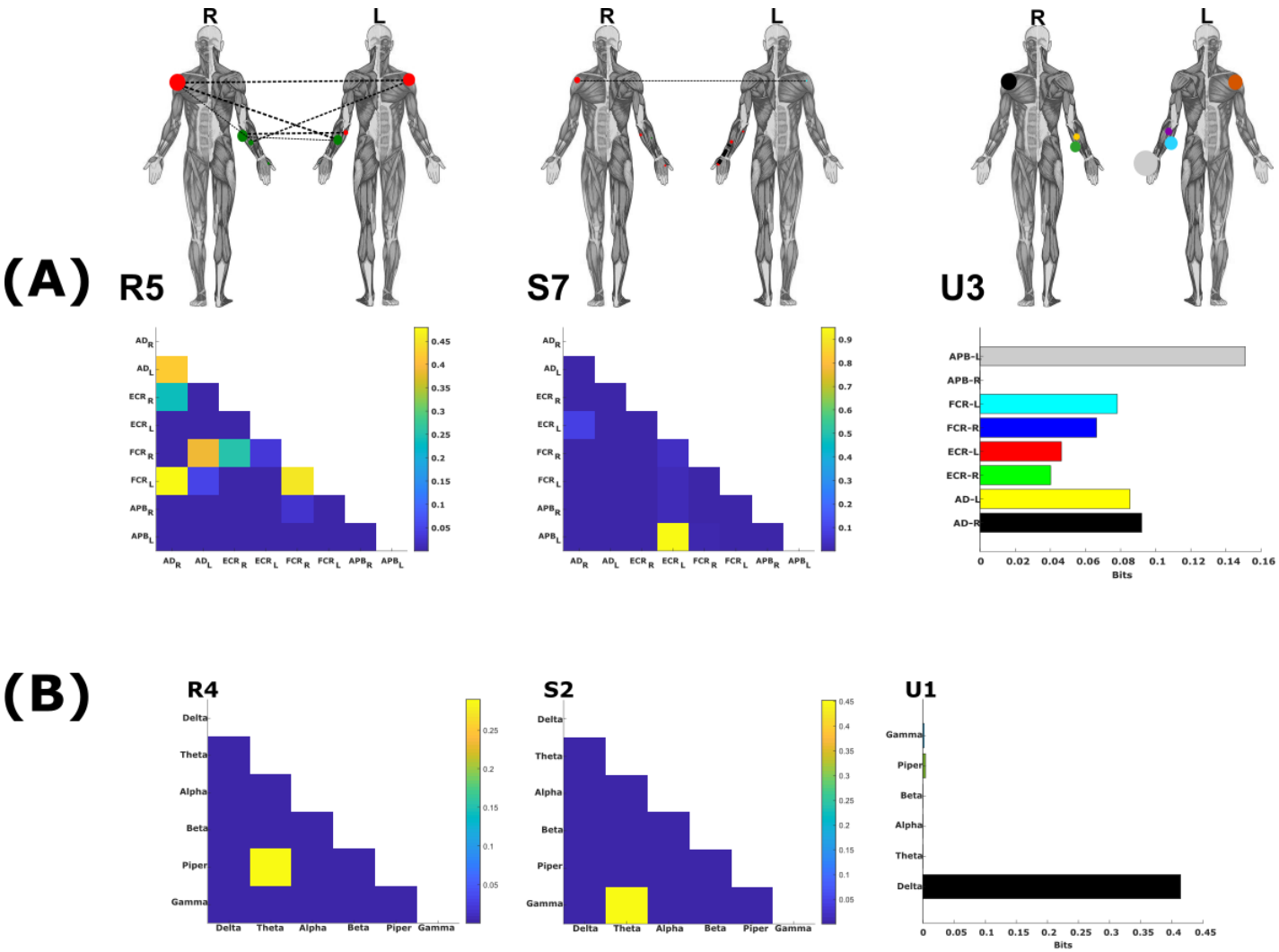

Fig.7: **(A)** The intermuscular components (R5, S7, U3) whose underlying recruitment variability ($\sum Error$) was significantly predictive of participants' age group. All three components formed part of a binary logistic regression model (R5: [β= -2.12±0.801, p<0.01], S7: [β= 1.36±0.704, p=0.053], U3: [β= 0.964±0.445, p<0.05]) and classified 75% of participants correctly. Above the adjacency matrices, human body models illustrate the network connectivity with relative edge width, node size and color representing the connection strength, muscle importance and sub-modularity [30,37,38]. **(B)** The intramuscular components (R4, S2, U1) whose underlying recruitment variability ($\sum Error$) was significantly predictive of participants' age group. All three components formed part of a binary logistic regression model (R4: [β= -0.557±0.313, p=0.075], S2: [β= -11.75±4.6, p=0.011], U1: [β= 1.94±0.982, p<0.05]) and classified 84.4% of participants correctly.

Discussion

In this study, we quantified and characterized functionally and hierarchically muscular interactions. We further demonstrated that they encode functionally relevant features of motor behavior. To this end, we proposed a novel approach to muscle synergy analysis that separately and simultaneously quantifies the redundant, synergistic and unique contributions of muscle interactions to task performance at both intermuscular (i.e. pairs of muscle activations) and intramuscular (i.e. pairs of rhythmic activities) levels. This approach builds on a previously established pipeline for the extraction of task-relevant muscle interaction patterns, going further by enabling the quantification of functional independence among individual muscles within these. Through the application of this framework to benchmark datasets, we firstly demonstrated how the decomposition of task-relevant muscle combinations reveals a complex functional architecture underlying everyday human movements. This functional architecture displayed a nested network structure of functionally similar and complementary information processing between muscles along with the unique contribution of individual muscles to task performance. We then investigated the contribution of individual muscles to task performance by applying the proposed framework to the intramuscular level, revealing that functional modularity is a scale-invariant characteristic fundamental to movement construction. We found that the extracted inter- and intra-muscular components were consistently generalizable

beyond any data subset and across disparate motor tasks such as whole-body reaching and balancing tasks. Finally, we showed that these motor components were differentially predictive of salient motor features including motor adaptation and age group, suggesting they offer complementary windows in movement control. Thus, we present the proposed framework as a powerful tool for fundamental mechanistic investigations with a novel lens into human action. As demonstrated here, this analytical tool can be used to a) characterize the functional outcomes of muscle interactions and compare them across populations or conditions and conversely b) identify physiological markers of motor performance, learning or impairment.

The proposed methodology aligns with recent theoretical innovations in the motor control research field that propose functional modularity both within- and between muscles as a mechanism for simplified and flexible movement control [18]. Within this theoretical framework, motoneurons affiliated with overlapping functional groups may innervate the same or different muscles (Fig.1.2), while individual muscles can also be independently controlled concomitantly. This proposition implies a diverse range of muscular interactions including muscles working together towards functionally similar, complementary and independent task-goals [14,15,17]. By posing the degrees-of-freedom problem of coordinated movement as the problem of information sharing across muscle networks [11,42], our framework effectively reveals this hierarchical and diverse functional architecture. To further elaborate, the extracted motor components captured multiple, co-occurring subnetworks of muscles (or intramuscular rhythms) that formed overlapping functional groups. Several of these patterns were shared across interaction types (e.g. Supp. Fig. 1-3), indicating diverse information processing indeed occurred concomitantly within the same muscle networks. Many of these motor components were centrally defined or were more widespread across the body. These networks of functional muscle connectivity across the body are underpinned by polysynaptic communication pathways involving feedforward and feedback processes. Among these communication pathways, both the centralized and peripheral routing of task information globally integrates muscle functionality across the body while diffusive processes prevail locally, promoting a segregation of functional roles [20,43–45]. Moreover, the unique adherence of top-down and bottom-up motor processes to specific task features likely enhances the selectivity of sensorimotor representations and consequently the adaptability of movement control [46]. The further involvement of network communication models (e.g. network communicability used here for illustrative purposes only [32,38]) in future applications of the proposed framework may prove useful for understanding how motor signals are broadcast throughout the muscle space [47].

The separate quantification of unique, redundant, and synergistic task information proposed here brought about interesting insights into human motor control. For instance, we were able to identify the functional underpinnings of the characteristic increased motor variability with ageing. We found increased fluctuations in functionally complementary intermuscular couplings with age coincided with decreased fluctuations in synergistic channels intramuscularly with age also (Fig.7). Meanwhile, functionally redundant variations reduced and functionally independent channels consistently exhibited increased fluctuations across scales in the older adults group. These findings strongly contest the notion of increased motor variability with aging being simply a manifestation of motor noise, but in fact consisting of increased fluctuations in functionally integrative and independent information channels. This supports empirical work highlighting this compensatory mechanism of integration in individuals with age-related neurodegeneration [48]. Continuing, we were also able to show that diverse types of task information are not isolated to specific muscle rhythms but are dynamically generated by various oscillatory signals to meet task demands. Among intramuscular R, gamma amplitudes were repeatedly associated with improved balance performance across participants when coupled in a functionally similar way with alpha- and beta-bands (Fig.6(B)). The alpha and beta-bands have been the subject of focus in several studies showing their crucial role in muscle synergy generation and monitoring [49–51]. Here we add to this line of research by uncovering a potentially crucial role of higher gamma oscillations in movement control.

Despite the strong base of evidence demonstrating the capacity of the individual muscle to augment whole movement patterns [20,52,53], muscle synergy research has generally focused on muscle clustering. Our findings here support recent formal applications of the muscle synergy concept to the intramuscular level, where task-specific modules have been identified [24–26]. Of note, past research suggested that intramuscular modules represent spinal-level circuitry while the intermuscular space primarily captures supraspinal mechanisms [26]. Indeed, this observation is supported by work from several research groups using different analytical techniques [54–56]. Here, we consistently found that the intramuscular level represented aspects of motor behavior indicative of superior task performance and proficiency (Fig.6-7), while the intermuscular level mainly represented decrements in performance and compensatory mechanisms (Fig.6-7). This opposing pattern intuitively aligns with this recent work, as erroneous performance requires more frequent intervention by supraspinal mechanisms while more effective movement can be coordinated automatously by spinal circuitry. An exception to this pattern however lies in the independent control of muscles quantified here as unique task information which demonstrated a correlation with better task performance inter-muscularly (Fig.6(A)) and of which increased fluctuations were consistently related to older age across both scales (Fig.7). This independent control mechanism is likely invoked where coarse-grained control mechanisms are insufficient, allowing for the necessary selectivity to maintain task performance. This suggests that variability in independent control mechanisms both between and within muscles plays a

major role in the manifestation of (and/or compensation for) behavioral inconsistency among older adults. However, as other related work also proposed [16,17,50,54], our findings here (Fig.6-7) suggest that there is not a clear distinction between the neural substrates underlying inter- and intra-muscular dynamics, and that they likely reflect the contributions of multiple neural substrates simultaneously, together holistically representing the motor system in a scale-invariant manner. Finally, our findings also highlight the crucial role of the individual muscle level in movement organization and promote further investigations on modular control at this scale. Indeed, an interesting avenue for future research would be to investigate the causal emergence of intramuscular dynamics from intermuscular constraints and vice versa, with the aim of mapping out the hierarchical interactions underlying coordinated movement.

In conclusion, we have developed and successfully applied a novel computational framework for the extraction of functionally diverse muscular interactions across multiple scales. We were able to comprehensively characterize the functional underpinnings of several distinct motor tasks while ensuring physiological relevance and generalizability. This principled method further widens the scope of the muscle synergy concept, showing how muscles can work together redundantly, synergistically, and independently towards task performance. In doing so, we align current approaches to muscle synergy analysis with the forefront of theoretical work on movement modularity. Overall, our framework offers improved flexibility and opportunities to future investigations through novel perspectives on movement control.

Materials and methods

Quantifying functionally diverse muscular interactions

To decompose the information a pair of muscles $[m_x, m_y]$ (or frequencies-specific amplitudes $[f_x, f_y]$) carries about τ into redundant, synergistic and unique components, we implemented the PID framework [28,57,58]. PID stems from a related information-theoretic measure known as co-information (co-I) that, by contrasting the sum of shared task information in m_x and m_y each alone ($I(m_x;\tau) + I(m_y;\tau)$) against their joint task information ($I(m_x, m_y;\tau)$), quantifies their multivariate mutual information ($II(m_x; m_y;\ \tau)$) (Equation 1.1) [27]. co-I results in a single value representing either a net redundancy (negative co-I values) or net synergy (positive co-I values) across the system. PID builds on this by removing the conflation of redundancy and synergy evident in co-I through the decomposition of $I(m_x, m_y;\tau)$ (i.e. the JMI) into separate redundant ($\mathrm{R}(m_x{:}\, m_y;\tau)$) and synergistic ($S(m_x{:}\, m_y;\tau)$) information atoms and the unique task information provided by m_x ($U(m_x{:}\,\tau|m_y)$) and m_y ($U(m_y{:}\,\tau|m_x)$) (Equation 1.2).

$$-II(m_x; m_y;\ \tau) = I(m_x;\tau) + I(m_y;\tau) - I(m_x, m_y;\tau) \qquad \textit{Equation } 1.1$$

$$I(m_x, m_y;\ \tau) = \mathrm{R}(m_x{:}\, m_y;\tau) + U(m_x{:}\,\tau|m_y) + U(m_y{:}\,\tau|m_x) + S(m_x{:}\, m_y;\tau) \qquad \textit{Equation } 1.2$$

To perform PID here, we implemented a novel PID framework for Gaussian variables based on local information estimates that has proven useful in neuroscientific applications [28,39,59–61]. We generated a multiplexed view of the muscular interactions underlying human movement by applying this method to all unique $[m_x, m_y]$ (or $[f_x, f_y]$) and τ combinations for each participant. To make these separate computations directly comparable, we normalized each PID component by their collective sum total which is equal to the JMI [39]. The resulting redundancy, synergy and two unique information estimates collectively form four symmetric adjacency matrices (A) (i.e. $A^T A = I$) that represent the functionally similar, complementary or unique connectivities between muscles (frequencies) with respect to τ. When repeated across all available task variables τ and participants, A is a multiplex network of dimension [No.of $[m_x, m_y]$ x [No.of τ x No.of participants]]. Thus, by applying network-theoretic statistical tools to A, we can identify functional modules carrying the same type of task information (i.e. redundant, synergistic, unique) (fig.1.2).

Identifying significant muscle interactions and their modular structure

The percolation threshold (P_c) (i.e. a critical value specifying the probability of node connectivities occurring and at which large clusters and long-range connectivity begin to appear across a given network [62]) has proven to be a fundamental constraint in nervous system organization [1,6,63]. To identify the network connections in our framework that align with P_c, we employed a modified percolation analysis [6]. We applied this method to each layer of A, sparsifying the network with respect to the P_c expected from equivalently sized random networks by thresholding connectivities iteratively until the largest cluster in the network (the '*giant component*') begins to be affected (Fig.2(C)).

Following this, in previous applications of the NIF [19,29], to determine the optimal number of clusters to extract with dimensionality reduction, we have implemented community detection protocols suitable for multiplexed networks [30,64,65]. In the current study however, due to the highly nested structure found in A, just a single cluster was identified

using these established methods. Therefore, to determine the optimal modular structure within a multiplexed network of muscles with overlapping functional affiliations, we employed a link-based community detection protocol [31]. Specifically, we firstly normalize network edges within each layer of A ($A(i)$) with respect to their corresponding JMI [39], and then applied single-linkage hierarchical clustering. In doing so, we built dendrograms for each network layer describing the clustering of dependencies that is cut at a threshold determined by the maximum of the partition density (D) (Fig.2(D)), defined for a given partition of M links and N nodes into C subsets (Equation 2.1) [31]. Here, D is the average of the number of links in a subset (m_c) normalized by the possible maximum and minimum number of nodes with respect to the number of nodes those links touch (n_c). This computation essentially unravels the nested network structure of each layer in A, resulting in a set of binary adjacency matrices that represent whether a muscle belongs to an identified cluster or not.

$$D = \frac{2}{M}\sum_{c} m_c \frac{m_c - (n_c - 1)}{(n_c - 2)(n_c - 1)} \qquad Equation\ 2.1$$

We then sum across all of these computed matrices across all layers of A, resulting in a single aggregate graph. Finally, we then apply the conventional community detection method based on a modularity maximization cost-function known as the Q-statistic (Q) (Equation 2.2) [30,37]. For a given partition of the network, the Q-statistic compares the number of edges between node i and j (A_{ij}) and what would be expected from an equivalent random network (P_{ij}). In letting $\delta(g_i, g_j)$=1 if nodes i and j belong to the same group (g) and 0 otherwise, thus this measure penalises partitions with a low ratio of within vs without cluster dependencies [30,66]. The optimal cluster count to extract was defined as the partition that maximises this Q-statistic.

$$Q = \frac{1}{4m}\sum_{ij}\left(A_{ij} - P_{ij}\right)\delta(g_i, g_j) \qquad Equation\ 2.2$$

Extraction of low-dimensional motor components

Using the optimal cluster count derived a priori as the input parameter into dimensionality reduction, namely PNMF [33], we extracted low-dimensional components of motor behavior from muscle interactions of a specific type (i.e. redundant, synergistic or unique) across tasks and participants (Fig.2(E)). In the case of the intermuscular space, this input matrix (A) was of shape [No. of $[m_x, m_y]$ x [No. of τ x No. of Participants]], while for the intramuscular space, A had a dimensionality of [No. of $[f_x, f_y]$ x [No. of muscles x No. of τ x No. of Participants]]. As described in equation 3.1 for the jth module and single participant and task case, A is factorized into two components, $\boldsymbol{v}$ a vector of muscle weightings (m) of length equal to the number of unique muscle pairs (K) and corresponding activation coefficients (s). The extraction of the modules identified during model-rank specification is verifiable as shown in previous NIF applications [29]. We note here that for the aim of extracting motor components predictive of differences in the sampled population (see '*Hierarchies of functional muscle interactions capture distinct motor features'* in the results section), we input the normalized PID values into dimensionality reduction. However, for the aim of extracting generalizable motor components (see '*Generalizable components of functionally diverse muscular interactions'* and '*Functional modularity is scale-invariant across the human motor system'* of the results section), we input the non-normalized version of A into dimensionality reduction.

$$A = \begin{pmatrix} \boldsymbol{v}_j^{m^1} \\ \vdots \\ \boldsymbol{v}_j^{m^K} \end{pmatrix} . \begin{pmatrix} s_j & \cdots & s_j \end{pmatrix} \qquad Equation\ 3.1$$

Examining the generalizability of extracted motor components

To determine the generalizability of the extracted motor components, using Pearson's correlation we determined the similarity between the extracted motor components and equivalent components extracted from a subset of the input data (i.e. when an individual participant or task was removed). We carried out this procedure for all tasks and participants and then focused our analysis on the correlation between functionally equivalent motor components (>0.5 correlation). To summarize this comparison, we converted the remaining coefficients into Fisher's Z values, computed averages and standard deviations, and then reverted these values back to correlation coefficients.

Salient features of motor performance

To probe how functionally diverse inter- and intra-muscular interactions represent motor performance, we quantified ∑Error in specific ways for dataset 2 and 3 for use in separate statistical analyses.

For dataset 2, ∑Error was defined as the absolute cumulative error of the balance board parameter ($|\sigma|$) across the *n*th trial (Equation 4.1). σ was any deviation from 0 degrees of the balance board along the horizontal plane. Using a repeated measures correlation [40], associations between ∑Error and trial-specific activation coefficients from inter- and intra-muscular componenets were determined. For the intramuscular activation coefficients specifically, we averaged them across muscles to get a [No. of trials x No. of participants] size vector equivalent to the intermuscular coefficients.

For dataset 3, a binary variable representing participants' age group (Young=0 vs. Old=1) was used as the dependent variable in a binary logistic regression model. ∑Error, a measure of motor variability, was used as the predictors in this model. ∑Error was defined as the absolute cumulative sum across trials of an inter- or intra-muscular activation coefficient σ demeaned with respect to their condition-specific average (i.e. light vs heavy objects) (Equation 4.1).

$$\sum Error = \sum_{n} |\sigma| \qquad Equation\ 4.1$$

We calculated ∑Error of all inter- and intra-muscular components and input these as predictors of age group in the logistic regression model. An optimally parsimonious model, including the minimal number of predictors, was determined using forward selection via the Wald's test criterion (inclusion: $p<0.05$, exclusion: $p>0.1$).

Subnetwork analysis

To illustrate the relative importance of individual muscles on the depicted human body models [36], we determined the total communicability ($C(i)$) of individual nodes (i) [38]. $C(i)$ is defined as the row-wise sum of all matrix exponentials (e) in the adjacency matrix (A) that consider the number of walks between each pair of nodes i and j (Equation 5.1) [32,38].

$$C(i) = \sum_{j=1}^{N} [e^{A}]_{ij} \qquad Equation\ 5.1$$

To emphasize salient functional connectivities present in the motor components, we further sparsified all dependencies with a below average network communicability and illustrated the output on the accompanying human body models [32,36]. To uncover salient subnetwork structures consisting of more closely functionally related muscles (indicated by node color on the human body model), we applied the community detection algorithm described in equation 2.3 to the extracted motor components [30,37].

Data acquisition and experimental conditions

To illustrate our framework, we applied it to four datasets of EMG signals and corresponding continuous task parameters recorded while human participants performed different motor tasks. In dataset 1 (fig.3(a)) [34], 3 healthy, adult participants performed whole-body, unimanual point-to-point reaching movements in various directions and to varying heights while EMG from 30 muscles (tibialis anterior, soleus, peroneus, gastrocnemius, vastus lateralis, rectus femoris, biceps femoris, gluteus maximus, erector spinae, pectoralis major, trapezius, anterior deltoid, posterior deltoid, biceps and triceps brachii) across both hemibodies were captured (Fig.3(a)). Alongside these EMG recordings, 3D kinematic data from 18 body locations (elbow, wrist, mid-arm, index finger, shoulder, hip, knee, ankle and foot) across both hemibodies were captured along with additional kinematics from the head, right eye, left ear, and the center of pressure. Participants performed ~2160 pseudo randomized trials each in structured blocks across two days to avoid fatigue. Movement onsets and offsets were determined at the timepoints which the index finger kinematic was 5% above and below its peak velocity in the trial respectively.

In dataset 2 (fig.3(b)), 3 healthy participants performed 10 consecutive trials of balancing on a balance board (Model 16130 Stability Platform, Lafayette Instrument) while self-induced perturbations were experienced along the frontal plane. Each trial lasted 30 seconds in which participants were instructed to maintain a balance board position parallel to the floor as best they could while focusing ahead at eye-level on a dot on the wall (<5 meters distance). Between trials, participants had 1 minute to rest. EMG recordings (Delsys Trigno™ wireless EMG, sampling frequency: 2000Hz) were taken from the bilateral medial gastrocnemius (MGN), tibialis anterior (TA), rectus femoris (RF) and biceps femoris (BF) while the horizontal angular displacement of the balance board was simultaneously recorded. Ethical approval was given by the Faculty of Biological Sciences Ethical Review Committee, University of Leeds.

For dataset 3 (fig.3(c)) [35], 14 young adults (22.1±2.4 years old, two left-handed, two males) and 18 older adults (71.6±6.9 years old, two left-handed, 8 males) performed a bimanual grasp-lift-hold-replace task of both a light (0.2kg) and heavy (0.4kg) object (two manipulanda made from carbon-filled nylon) while in a seated position in front of a table. The objects were placed on the table 75% of shoulder width and 70% of maximum reach for each participant who were instructed to grasp the object and lift it to a target height in front of them (300mm height) and to hold the object as still as possible at this position for 10 seconds. Following this holding period, the participant was instructed to replace the object(s) back on the starting position markers. Participants performed 10 consecutive repetitions for each weight condition while EMG signals from the bilateral anterior deltoid (AD), extensor carpi radialis (ECR), flexor carpi radialis (FCR) and abductor pollicis brevis (APB) were recorded (Delsys Trigno™, sampling frequency: 2000Hz). Grip forces were recorded from 50N load cells (Omega, LCM201-50), acquired from a 16-bit data acquisition card (National Instruments, USB-6002) and processed in Labview (v.1.4). For load forces, six degree-of-freedom models were created in Qualisys for each object and were used to compute their 3D acceleration from which net load forces were calculated with respect to object mass. Trials commenced from 100ms prior to first contact until 100ms after last point of contact of either hand with the object, determined via recorded kinematic data of the objects position.

Data pre-processing

Intermuscular analyses

The processing of EMG signals from dataset 1 and 2 for the purpose of analyses in the intermuscular space included the application of a bidirectional low-pass Butterworth filter with zero-phase distortion (order: 4th, cut-off: 20Hz) to the rectified signals. Extrapolation of the kinematic data for dataset 1 and 2 to align with the corresponding EMG signals was carried out using a cubic spline method. For dataset 3, the signals were processed as described in [35]. More specifically, the rectified EMG signals were low-pass filtered (filter: 4th order Butterworth with zero-phase distortion, cut-off: 10Hz) and down-sampled to 200Hz to align with kinetic and kinematic datapoints. The filtered EMG signals were then normalized against their peak amplitudes across trials. The grip and load forces were smoothed using a low-pass filter (cut-off: 12Hz, filter: 4th order Butterworth).

Intramuscular analyses

The processing of EMG signals for the purpose of intramuscular analyses in the intramuscular space were uniform across datasets 1-3. This processing firstly included the filtration of the raw, unrectified EMG signals into specific frequency bands (Delta [0.1-4 Hz], Theta [4-8 Hz], Alpha [8-12 Hz], Beta [12-30 Hz], Low-Gamma (Piper rhythm) [30-60 Hz], High Gamma (Gamma) [60-80 Hz]) using a low- and high-pass filter combination (bi-directional 4th order Butterworth filters with zero-phase distortion). Then the absolute values from a Hilbert transform of the filtered signals representing their oscillatory amplitudes were extracted for further analysis. In the case of dataset 3, no down-sampling of the EMG signals occurred as carried out for intermuscular analyses. The task parameters for datasets 1-3 were all extrapolated using a cubic spline method to temporally align with the corresponding, processed EMGs and no further processing was carried out.

Author contributions

DOR: Methodological development, conceptual development, coding, testing, data curation (Dataset 2), processing and framework application, manuscript writing and editing.
WS: Data curation (Dataset 3).
PH: Data curation (Dataset 1), manuscript review.
RA: Data curation (Dataset 2), Data pre-processing, manuscript review.
SA: Data curation (Dataset 3), manuscript review.
ID: Supervision, conceptual and methodological development, manuscript editing.

Acknowledgments

We would like to thank Daniel Chicharro for the helpful discussions on Partial Information Decompositions.

References

[1] Gallos LK, Sigman M, Makse HA. The Conundrum of Functional Brain Networks: Small-World Efficiency or Fractal Modularity. Front Physiol 2012;3. https://doi.org/10.3389/fphys.2012.00123.

[2] Bullinaria JA. Understanding the Emergence of Modularity in Neural Systems. Cognitive Science 2007;31:673–95. https://doi.org/10.1080/15326900701399939.

[3] Levin M. Collective Intelligence of Morphogenesis as a Teleonomic Process 2022. https://doi.org/10.31234/osf.io/hqc9b.

[4] Ivanenko YP, Poppele RE, Lacquaniti F. Five basic muscle activation patterns account for muscle activity during human locomotion. J Physiol 2004;556:267–82. https://doi.org/10.1113/jphysiol.2003.057174.
[5] Nigam S, Pojoga S, Dragoi V. Synergistic Coding of Visual Information in Columnar Networks. Neuron 2019;104:402-411.e4. https://doi.org/10.1016/j.neuron.2019.07.006.
[6] Gallos LK, Makse HA, Sigman M. A small world of weak ties provides optimal global integration of self-similar modules in functional brain networks. PNAS 2012;109:2825–30. https://doi.org/10.1073/pnas.1106612109.
[7] Griffith V, Koch C. Quantifying synergistic mutual information. Guided self-organization: inception, Springer; 2014, p. 159–90.
[8] Perrone P, Ay N. Hierarchical Quantification of Synergy in Channels. Frontiers in Robotics and AI 2016;2.
[9] Salmas P, Cheung VCK. Gradient descent decomposition of force-field motor primitives optogenetically elicited for motor mapping of the murine lumbosacral spinal cord. Zr 2023;44:604–19. https://doi.org/10.24272/j.issn.2095-8137.2022.276.
[10] Latash ML. Synergy. Oxford University Press; 2008.
[11] Bernstein NA. The Co-ordination and Regulation of Movements. PergamonPress Ltd., Headington Hill Hall. Oxford; 1967.
[12] Bruton M, O'Dwyer N. Synergies in coordination: a comprehensive overview of neural, computational, and behavioral approaches. Journal of Neurophysiology 2018;120:2761–74. https://doi.org/10.1152/jn.00052.2018.
[13] Bizzi E, Cheung VC. The neural origin of muscle synergies. Front Comput Neurosci 2013;7. https://doi.org/10.3389/fncom.2013.00051.
[14] Hug F, Del Vecchio A, Avrillon S, Farina D, Tucker K. Muscles from the same muscle group do not necessarily share common drive: evidence from the human triceps surae. Journal of Applied Physiology 2021;130:342–54. https://doi.org/10.1152/japplphysiol.00635.2020.
[15] Hug F, Avrillon S, Sarcher A, Del Vecchio A, Farina D. Correlation networks of spinal motor neurons that innervate lower limb muscles during a multi-joint isometric task. The Journal of Physiology n.d.;n/a. https://doi.org/10.1113/JP283040.
[16] Alessandro C, Barroso FO, Prashara A, Tentler DP, Yeh H-Y, Tresch MC. Coordination amongst quadriceps muscles suggests neural regulation of internal joint stresses, not simplification of task performance. PNAS 2020;117:8135–42. https://doi.org/10.1073/pnas.1916578117.
[17] Vecchio AD, Germer C, Kinfe TM, Nuccio S, Hug F, Eskofier B, et al. Common synaptic inputs are not distributed homogeneously among the motor neurons that innervate synergistic muscles 2022:2022.01.23.477379. https://doi.org/10.1101/2022.01.23.477379.
[18] Hug F, Avrillon S, Ibáñez J, Farina D. Common synaptic input, synergies and size principle: Control of spinal motor neurons for movement generation. The Journal of Physiology 2023;601:11–20.
[19] Reilly DÓ, Delis I. Dissecting muscle synergies in the task space 2023:2023.03.17.533096. https://doi.org/10.1101/2023.03.17.533096.
[20] Dimitriou M. Human muscle spindles are wired to function as controllable signal-processing devices. eLife 2022;11:e78091. https://doi.org/10.7554/eLife.78091.
[21] Formento E, Botros P, Carmena JM. Skilled independent control of individual motor units via a non-invasive neuromuscular–machine interface. J Neural Eng 2021;18:066019. https://doi.org/10.1088/1741-2552/ac35ac.
[22] Basmajian JV. Control and training of individual motor units. Science 1963;141:440–1. https://doi.org/10.1126/science.141.3579.440.
[23] Aeles J, Horst F, Lapuschkin S, Lacourpaille L, Hug F. Revealing the unique features of each individual's muscle activation signatures. Journal of The Royal Society Interface 2021;18:20200770. https://doi.org/10.1098/rsif.2020.0770.
[24] Madarshahian S, Letizi J, Latash ML. Synergic control of a single muscle: The example of flexor digitorum superficialis. The Journal of Physiology 2021;599:1261–79.
[25] Madarshahian S, Latash ML. Synergies at the level of motor units in single-finger and multi-finger tasks. Exp Brain Res 2021;239:2905–23. https://doi.org/10.1007/s00221-021-06180-y.
[26] Madarshahian S, Latash ML. Effects of hand muscle function and dominance on intra-muscle synergies. Human Movement Science 2022;82:102936. https://doi.org/10.1016/j.humov.2022.102936.
[27] McGill W. Multivariate information transmission. Transactions of the IRE Professional Group on Information Theory 1954;4:93–111.

[28] Ince RAA. Measuring Multivariate Redundant Information with Pointwise Common Change in Surprisal. Entropy 2017;19:318. https://doi.org/10.3390/e19070318.
[29] Reilly DÓ, Delis I. A network information theoretic framework to characterise muscle synergies in space and time. J Neural Eng 2022;19:016031. https://doi.org/10.1088/1741-2552/ac5150.
[30] Blondel VD, Guillaume J-L, Lambiotte R, Lefebvre E. Fast unfolding of communities in large networks. J Stat Mech 2008;2008:P10008. https://doi.org/10.1088/1742-5468/2008/10/P10008.
[31] Ahn Y-Y, Bagrow JP, Lehmann S. Link communities reveal multiscale complexity in networks. Nature 2010;466:761–4. https://doi.org/10.1038/nature09182.
[32] Estrada E, Hatano N. Communicability in complex networks. Phys Rev E Stat Nonlin Soft Matter Phys 2008;77:036111. https://doi.org/10.1103/PhysRevE.77.036111.
[33] Yuan Z, Yang Z, Oja E. Projective Nonnegative Matrix Factorization: Sparseness, Orthogonality, and Clustering n.d.:14.
[34] Hilt PM, Delis I, Pozzo T, Berret B. Space-by-Time Modular Decomposition Effectively Describes Whole-Body Muscle Activity During Upright Reaching in Various Directions. Front Comput Neurosci 2018;12. https://doi.org/10.3389/fncom.2018.00020.
[35] Ye C, Saboksayr SS, Shaw W, Coats RO, Astill SL, Mateos G, et al. A Tensor Decomposition Uncovers the Effect of Ageing on Muscle and Grip-Load Force Couplings During Grasping 2022:2022.02.25.482040. https://doi.org/10.1101/2022.02.25.482040.
[36] Makarov SN, Noetscher GM, Nazarian A. Low-Frequency Electromagnetic Modeling for Electrical and Biological Systems Using MATLAB. John Wiley & Sons; 2015.
[37] Rubinov M, Sporns O. Complex network measures of brain connectivity: uses and interpretations. Neuroimage 2010;52:1059–69. https://doi.org/10.1016/j.neuroimage.2009.10.003.
[38] Benzi M, Klymko C. Total communicability as a centrality measure. Journal of Complex Networks 2013;1:124–49. https://doi.org/10.1093/comnet/cnt007.
[39] Daube C, Ince RAA, Gross J. Simple Acoustic Features Can Explain Phoneme-Based Predictions of Cortical Responses to Speech. Current Biology 2019;29:1924-1937.e9. https://doi.org/10.1016/j.cub.2019.04.067.
[40] Bakdash JZ, Marusich LR. Repeated Measures Correlation. Frontiers in Psychology 2017;8.
[41] Hunter SK, Pereira HM, Keenan KG. The aging neuromuscular system and motor performance. Journal of Applied Physiology 2016;121:982–95. https://doi.org/10.1152/japplphysiol.00475.2016.
[42] Schneidman E, Bialek W, Berry MJ. Synergy, Redundancy, and Independence in Population Codes. J Neurosci 2003;23:11539–53. https://doi.org/10.1523/JNEUROSCI.23-37-11539.2003.
[43] Ronzano R, Skarlatou S, Barriga BK, Bannatyne BA, Bhumbra GS, Foster JD, et al. Spinal premotor interneurons controlling antagonistic muscles are spatially intermingled. eLife 2022;11:e81976. https://doi.org/10.7554/eLife.81976.
[44] van den Heuvel MP, Kahn RS, Goñi J, Sporns O. High-cost, high-capacity backbone for global brain communication. Proceedings of the National Academy of Sciences 2012;109:11372–7. https://doi.org/10.1073/pnas.1203593109.
[45] Avena-Koenigsberger A, Misic B, Sporns O. Communication dynamics in complex brain networks. Nat Rev Neurosci 2018;19:17–33. https://doi.org/10.1038/nrn.2017.149.
[46] Johansson RS, Flanagan JR. Coding and use of tactile signals from the fingertips in object manipulation tasks. Nat Rev Neurosci 2009;10:345–59. https://doi.org/10.1038/nrn2621.
[47] Seguin C, Mansour L S, Sporns O, Zalesky A, Calamante F. Network communication models narrow the gap between the modular organization of structural and functional brain networks. NeuroImage 2022;257:119323. https://doi.org/10.1016/j.neuroimage.2022.119323.
[48] Pathak A, Sharma V, Roy D, Banerjee A. Biophysical mechanism underlying compensatory preservation of neural synchrony over the adult lifespan. Commun Biol 2022;5:1–12. https://doi.org/10.1038/s42003-022-03489-4.
[49] Zandvoort CS, van Dieën JH, Dominici N, Daffertshofer A. The human sensorimotor cortex fosters muscle synergies through cortico-synergy coherence. NeuroImage 2019;199:30–7. https://doi.org/10.1016/j.neuroimage.2019.05.041.
[50] Zipser-Mohammadzada F, Conway BA, Halliday DM, Zipser CM, Easthope CA, Curt A, et al. Intramuscular coherence during challenging walking in incomplete spinal cord injury: Reduced high-frequency coherence reflects impaired supra-spinal control. Frontiers in Human Neuroscience 2022;16.
[51] Laine CM, Cohn BA, Valero-Cuevas FJ. Temporal control of muscle synergies is linked with alpha-band neural drive. The Journal of Physiology 2021;599:3385–402.

[52] Kargo WJ, Giszter SF. Individual Premotor Drive Pulses, Not Time-Varying Synergies, Are the Units of Adjustment for Limb Trajectories Constructed in Spinal Cord. J Neurosci 2008;28:2409–25. https://doi.org/10.1523/JNEUROSCI.3229-07.2008.
[53] Cheung VCK, d'Avella A, Tresch MC, Bizzi E. Central and Sensory Contributions to the Activation and Organization of Muscle Synergies during Natural Motor Behaviors. J Neurosci 2005;25:6419–34. https://doi.org/10.1523/JNEUROSCI.4904-04.2005.
[54] Zandvoort CS, Daffertshofer A, Dominici N. Cortical contributions to locomotor primitives in toddlers and adults. Iscience 2022;25:105229.
[55] Overduin SA, d'Avella A, Roh J, Carmena JM, Bizzi E. Representation of muscle synergies in the primate brain. Journal of Neuroscience 2015;35:12615–24.
[56] Schouenborg J. Action-based sensory encoding in spinal sensorimotor circuits. Brain Research Reviews 2008;57:111–7.
[57] Williams PL, Beer RD. Nonnegative decomposition of multivariate information. arXiv Preprint arXiv:10042515 2010.
[58] Timme N, Alford W, Flecker B, Beggs JM. Synergy, redundancy, and multivariate information measures: an experimentalist's perspective. J Comput Neurosci 2014;36:119–40. https://doi.org/10.1007/s10827-013-0458-4.
[59] Ince RAA, Giordano BL, Kayser C, Rousselet GA, Gross J, Schyns PG. A statistical framework for neuroimaging data analysis based on mutual information estimated via a gaussian copula. Hum Brain Mapp 2016;38:1541–73. https://doi.org/10.1002/hbm.23471.
[60] Delis I, Ince RAA, Sajda P, Wang Q. Neural Encoding of Active Multi-Sensing Enhances Perceptual Decision-Making via a Synergistic Cross-Modal Interaction. J Neurosci 2022;42:2344–55. https://doi.org/10.1523/JNEUROSCI.0861-21.2022.
[61] Park H, Ince RAA, Schyns PG, Thut G, Gross J. Representational interactions during audiovisual speech entrainment: Redundancy in left posterior superior temporal gyrus and synergy in left motor cortex. PLOS Biology 2018;16:e2006558. https://doi.org/10.1371/journal.pbio.2006558.
[62] Li M, Liu R-R, Lü L, Hu M-B, Xu S, Zhang Y-C. Percolation on complex networks: Theory and application. Physics Reports 2021;907:1–68. https://doi.org/10.1016/j.physrep.2020.12.003.
[63] Razban RM, Pachter JA, Dill KA, Mujica-Parodi LR. Early path dominance as a principle for neurodevelopment. Proceedings of the National Academy of Sciences 2023;120:e2218007120. https://doi.org/10.1073/pnas.2218007120.
[64] Mucha PJ, Richardson T, Macon K, Porter MA, Onnela J-P. Community Structure in Time-Dependent, Multiscale, and Multiplex Networks. Science 2010;328:876–8. https://doi.org/10.1126/science.1184819.
[65] Didier G, Brun C, Baudot A. Identifying communities from multiplex biological networks. PeerJ 2015;3:e1525. https://doi.org/10.7717/peerj.1525.
[66] Newman MEJ, Girvan M. Finding and evaluating community structure in networks. Phys Rev E 2004;69:026113. https://doi.org/10.1103/PhysRevE.69.026113.